論文 / 著書情報
Article / Book Information

Title	Three-dimensional resistivity structure and magma plumbing system of the Kirishima volcanoes as inferred from broad-band magnetotelluric data
Author	Aizawa, K., Koyama, T., Hase, H., Uyeshima, M., Kanda, W., Utsugi, M., Yoshimura, R., Yamaya, Y., Hashimoto, T., Yamazaki, K., Komatsu, S., Watanabe, A., Miyakawa, K., Ogawa, Y.
Journal/Book name	Journal of Geophysical Research: Solid Earth, 119, , 198–215
Issue date	2014, 1
DOI	http://dx.doi.org/10.1002/2013JB010682
権利情報 / Copyright	Copyright (c) 2014 American Geophysical Union (AGU)

AGU PUBLICATIONS

JGR

Journal of Geophysical Research: Solid Earth

RESEARCH ARTICLE
10.1002/2013JB010682

Key Points:
- First 3-D inversion of the anomalous magnetotelluric data
- Comparison of the structure with deformation source and seismicity
- Magma plumbing system deduced from above comparison

Correspondence to:
K. Aizawa,
aizawa@sevo.kyushu-u.ac.jp

Citation:
Aizawa, K., et al. (2014), Three-dimensional resistivity structure and magma plumbing system of the Kirishima Volcanoes as inferred from broadband magnetotelluric data, *J. Geophys. Res. Solid Earth*, *119*, doi:10.1002/2013JB010682.

Received 12 SEP 2013
Accepted 7 DEC 2013
Accepted article online 18 DEC 2013

Three-dimensional resistivity structure and magma plumbing system of the Kirishima Volcanoes as inferred from broadband magnetotelluric data

Koki Aizawa[1,2], Takao Koyama[1], Hideaki Hase[1,3], Makoto Uyeshima[1], Wataru Kanda[3], Mitsuru Utsugi[4], Ryokei Yoshimura[5], Yusuke Yamaya[1,6], Takeshi Hashimoto[7], Ken'ichi Yamazaki[8], Shintaro Komatsu[8], Atsushi Watanabe[1], Koji Miyakawa[1], and Yasuo Ogawa[3]

[1]Earthquake Research Institute, University of Tokyo, Tokyo, Japan, [2]Institute of Seismology and Volcanology, Faculty of Sciences, Kyushu University, Shimabara, Japan, [3]Volcanic Fluid Research Center, Tokyo Institute of Technology, Tokyo, Japan, [4]Aso Volcanological Laboratory, Institute for Geothermal Sciences, Graduate School of Science, Kyoto University, Kumamoto, Japan, [5]Disaster Prevention Research Institute, Kyoto University, Uji, Japan, [6]Geological Survey of Japan, National Institute of Advanced Industrial Science and Technology, Tsukuba, Japan, [7]Institute of Seismology and Volcanology, Faculty of Science, Hokkaido University, Sapporo, Japan, [8]Miyazaki Observatory, Disaster Prevention Research Institute, Kyoto University, Miyazaki, Japan

Abstract Broadband magnetotelluric (MT) measurements were conducted in 2010 and 2011 in the vicinity of Shinmoe-dake Volcano in the Kirishima volcano group, Japan, where sub-Plinian eruptions took place 3 times during 26–27 January 2011. By combining the new observations with previous MT data, it is found that an anomalous phase in excess of 90° is commonly observed in the northern sector of the Kirishima volcano group. Because the anomalous phase is not explained by 1-D or 2-D structure with isotropic resistivity media, 3-D inversions were performed. By applying small errors to the anomalous phase, we successfully estimated a 3-D resistivity structure that explains not only the normal data but also the anomalous phase data. The final model shows a vertical conductor that is located between a deep-seated conductive body (at a depth greater than 10 km) and a shallow conductive layer. By applying the findings of geophysical and petrological studies of the 2011 sub-Plinian eruptions, we infer that the subvertical conductor represents a zone of hydrothermal aqueous fluids at temperatures over 400°C, in which a magma pathway (interconnected melt) is partially and occasionally formed before magmatic eruptions. To the north of the deep conductor, earthquake swarms occurred from 1968 to 1969, suggesting that these earthquakes were caused by volcanic fluids.

1. Introduction

In the southern part of Kyushu Island, Japan, the Philippine Sea Plate subducts to the WNW at a rate of approximately 5 cm/yr [*Seno et al.*, 1993]. In this area, active volcanoes with large calderas are distributed along a north–south trending volcanic chain (Figure 1). The Kirishima volcano group (the Kirishima Volcanoes) is situated at the northernmost end of the southern Kyushu volcanic chain and consists of more than 20 Quaternary volcanic cones within an area of ~20 × 30 km. Two calderas (Kakuto and Kobayashi) are located in the northern sector of the Kirishima Volcanoes, where some 100 km^3 of magma was extruded between ~300 and ~500 kyr ago [*Tajima and Aramaki*, 1980; *Imura*, 1994].

The Kirishima volcano group started to increase in extent after the formation of the calderas. Although the volcanic cones are distributed roughly from NW to SE, a systematic shift of the eruption center is not recognized in its 300 kyr history (i.e., volcanic cones seem to be randomly located); therefore, the locations of magma chambers are not indicated from geological studies. Beneath the Kakuto caldera, five earthquake swarms have been observed since 1913 [*Miyazaki et al.*, 1976]. The 1968–1969 events were characterized by more than 5000 earthquakes at a depth of 3–9 km, with a largest magnitude of 6.1 [*Minakami et al.*, 1969]. To investigate the relationship between earthquakes and volcanic fluid (presumably magma beneath Kakuto caldera), *Goto et al.* [1997] conducted a series of broadband magnetotelluric (MT) surveys. However, the authors discovered that the hypocentral area is in fact highly resistive and considered it unlikely that a large mass of fluid is located in the hypocentral area.

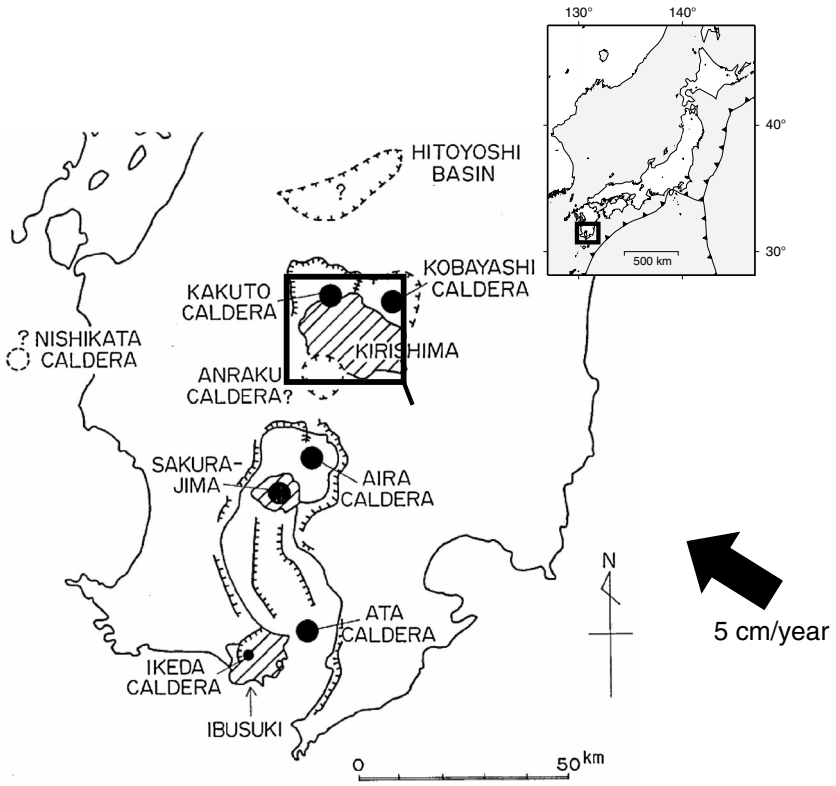

Figure 1. Map showing the locations of major calderas and active volcanoes in southern Kyusyu, Japan (taken from *Tajima and Aramaki* [1980]). Inset shows the location of the figure within Japan. Solid circles indicate inferred positions of the vents of pyroclastic flows related to caldera formation. Hatched areas are active volcanoes. The solid rectangle indicates the area of Figure 2. The arrow shows the subduction direction of the Philippine Sea Plate.

The most recent eruptions of the Kirishima Volcanoes occurred in the central and southeastern sectors of the group. Since AD 742, documented eruptions have taken place at three volcanoes: Iwo-Yama (altitude 1310 m), Shinmoe-dake (1421 m), and Ohachi (1408 m) (Figure 2). Since the 1923 eruption of Ohachi Volcano, all other eruptions (i.e., the 1959, 1962, 1991, 2010, and 2011 eruptions) have occurred at Shinmoe-dake Volcano [*Imura and Kobayashi*, 1991; *Tsutsui et al*., 2005; *Nakada et al*., 2013], with the 2011 eruptions being the largest on record in the group since a similar-scale eruption at Shinmoe-dake in 1717. The 2011 event started with a series of small eruptions between 19 and 22 January, followed by three sub-Plinian eruptions during 26–27 January and the subsequent emergence of lava within the crater [*Nakada et al*., 2013]. Synchronous with the sub-Plinian eruptions, tiltmeters, and global positioning system instruments detected ground subsidence in an area located approximately 7 km WNW of Shinmoe-dake (Figure 2), at an estimated source depth of ~10 km [*Kozono et al*., 2013; *Nakao et al*., 2013; *Ueda et al*., 2013]. The estimated volume of the deflation was about 0.016 km^3 [*Kozono et al*., 2013; *Ueda et al*., 2013], which is within 1 order of magnitude of the amount of erupted material observed (0.021–0.027 km^3 dense rock equivalent [*Nakada et al*., 2013]). At approximately the same location as the syn-eruptive deflation, inflation was observed from February 2010 to January 2011 and from February 2011 to October 2011, which suggests that magma had accumulated at the source of the deformation both before and after the late January 2011 eruptions [*Nakao et al*., 2013].

The 2011 syn-eruptive ground subsidence is regarded as clear evidence of subsurface magma migration, and its characteristics have been studied in detail. Significantly, a time lag was not detected between the subsidence and the development of the eruption plumes [*Kozono et al*., 2013]. This suggests that a magma pathway existed prior to the 2011 sub-Plinian eruptions. The existence of such a pathway is also supported by the fact that the precursory increase in seismicity was not observed in advance of the 2011 sub-Plinian eruptions.

Although the magma pathway has not been imaged, some studies have investigated various aspects of the magma chamber beneath the Kirishima Volcanoes. Based on hypocenter distributions, *Ida et al*. [1986]

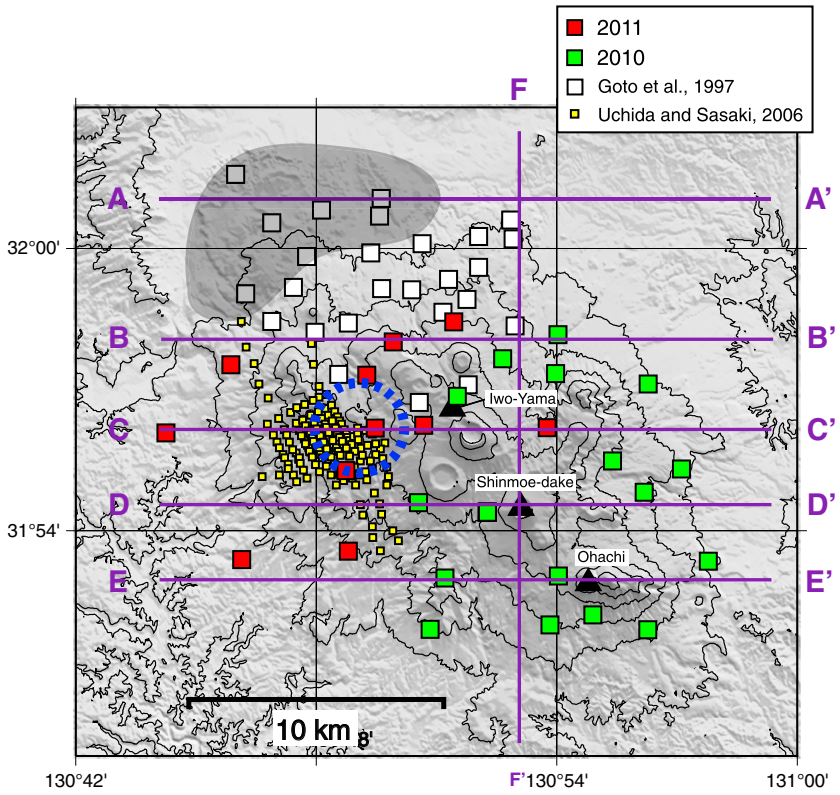

Figure 2. Broadband magnetotelluric (MT) observation sites at the Kirishima volcano group. The topographic contour interval is 200 m. The hypocentral area of the 1968–1969 Ebino earthquake swarm, whose epicenter depth is 3–9 km [*Minakami et al*., 1969], is represented by the shaded grey area. The dashed blue circle indicates the possible location of the syn-eruptive deformation source (*Ueda et al*., 2013; *Kozono et al*., 2013). The blue lines indicate the locations of transects along which vertical slices (Figure 12) of the final 3-D resistivity structure were taken.

speculated that a magma chamber is located NW of the Kirishima Volcanoes. On the basis of magnetotelluric (MT) surveys using the ultralow frequency band (over 10 s) and 1-D inversion, *Utada et al*. [1994] and *Kagiyama et al*. [1997] suggested that magma does not exist beneath the SE sector of the Kirishima Volcanoes but does exist beneath the NW sector. *Yamamoto and Ida* [1997] studied the *P* wave seismic structure and found a high-attenuation zone located NW of the Kirishima Volcanoes at a depth of 5 km. From the frequency dependence of the attenuation, the authors suggested the existence of an 80 m thick sill-like magma body there. However, the spatial resolutions of these previous studies were coarse, as low as 4 km; consequently, the volume and shape of the magma chamber remain unknown. The possible magmatic pathway, which should connect the Shinmoe-dake crater and the source of deformation of the syn-eruptive ground subsidence, was not suggested by these previous studies.

In this study, we examine the 3-D resistivity structure of the Kirishima Volcanoes estimated using a broadband (0.003–2048 s) magnetotelluric (MT) data set. Compared with the previous MT survey [*Utada et al*., 1994], the MT data set covers a wider area and greater depth range, and we investigate from the deep magma chamber level up to the shallow hydrothermal system at high spatial resolution. Because melt [*Tyburczy and Waff*, 1983; *Gaillard and Marziano*, 2005] and saline water [*Nesbitt*, 1993] are both highly conductive, a broadband MT survey and 3-D data modeling are appropriate for investigating the magma and/or magmatic fluid upwelling under active volcanoes [*Hill et al*., 2009; *Ingham et al*., 2009; *Heise et al*., 2010; *Bertrand et al*., 2012; *Kelbert et al*., 2012].

2. MT Observations

From July to August 2010 and March to April 2011, we recorded naturally occurring geomagnetic fields (B_x, B_y, and B_z) and induced Earth electric fields (E_x and E_y) at 28 broadband MT observation sites (Figure 2) using

a Metronix ADU07 system. The sampling frequencies were set at 32 Hz (00:00–23:50 UT) and 1024 Hz (17:00–18:00 UT). The typical record duration was 2 weeks for one site. In addition to our surveys, previous broadband MT data [*Goto et al*., 1997; *Uchida and Sasaki*, 2006], which were recorded by Phoenix V5 and MTU5 systems, were used in this study. Taking into account that the erupted volume of magma is on the order of 0.01 km^3, we assume that the resistivity structure has not significantly changed since those observations were made. Although the measurement sites in 2010 and 2011 do not overlap with the previous sites, the continuous MT observation at Iwo-Yama since May 2011 suggested that a resistivity change occurred only at a shallow level (less than several hundred meters) and its amplitude was subtle less than ±10% [*Aizawa et al*., 2013].

The survey of *Goto et al*. [1997] was conducted to examine the existence of fluid in the hypocentral area of the 1968–1969 Ebino earthquake swarms. By 2-D inversion, the authors concluded that the hypocentral area corresponded to a zone of high resistivity. The extremely dense broadband MT data of *Uchida and Sasaki* [2006] were obtained for exploration around the Ogiri geothermal power plant by the New Energy and Industrial Technology Development Organization, Nittetsu Kagoshima Geothermal Co., Ltd., and the Geological Survey of Japan during the period 1996–2000. By using the off-diagonal components of the impedance tensor in the period range 0.01–10 s, the authors imaged the 3-D resistivity structure to a depth of 4 km and suggested that high-temperature (above 200°C) hot water is trapped beneath the conductive cap rock located at 1 km depth.

3. Time Series Analysis

Although there are no electrical power lines near the MT sites, artificial 60 Hz noise (and associated odd-order overtones at 180, 300, and 420 Hz) originating from distant commercial power lines is still observed in the recorded power spectra of all five measured components (E_x, E_y, B_x, B_y, and B_z). Because ADU07 is not equipped with a notch filter, the commercial noise presents a serious problem to the estimation of MT response functions. To reduce this noise, we applied a digital notch filter. A raw time series of data was first transformed to the frequency domain by applying a Fourier transform with a time window of 2^{13} s. In this step, the data were multiplied by the frequency responses of the induction coil and logger. Then, the amplitudes of the 60 Hz odd-order overtones were reduced to 1/100 of their values, with a notch width of 0.1 Hz. Finally, the time series data with physical units of mV/km and nT were recovered using an inverse Fourier transform. By applying this comblike notch filter, the quality of MT response functions was significantly improved, especially at frequencies near 60 Hz and at odd-order overtones. We confirmed that the calculated MT response functions are robust against the slight change of filter parameters (notch width, reduce factor, and time window).

The MT response functions were calculated using a robust estimation code [*Chave and Thomson*, 2004]. At a period less than 10 s, we also employed remote reference processing [*Gamble et al*., 1979] using MT data recorded at other MT sites. At a period over 10 s, the 1 Hz-sampled geomagnetic data recorded at the Kakioka Magnetic Observatory (located 1000 km ENE of Kirishima) were used for remote reference processing. Using these procedures, we obtained the MT response functions across a broad period range of 0.003–2048 s.

The frequencies of the MT response functions in 2010–2011 differ slightly from the previous MT data due to the difference in sampling frequency. This discrepancy created problems for further analysis, including inversion. Because MT response functions are inherently smooth with frequencies, we interpolated the MT response functions and error bars of the previous data in the frequency domain by using a cubic spline function. The MT response functions were then defined at the frequencies for 2010–2011.

4. Characteristics of the Data (Anomalous Phase in Excess of 90°)

Before inversion was performed, the characteristics of the MT data were examined. Because the data around the Ogiri geothermal power plant [*Uchida and Sasaki*, 2006] are too dense to analyze (Figure 2), we picked nine sites from these data. Figure 3a shows a map of the phase at a period of 512 s. The phase for Z_{xy} shows higher values than Z_{yx} and exceeds 90° in the northern sector of the Kirishima Volcanoes. Note that Z_{yx} phases are quite normal (0–90°) at all periods. Figure 3b shows an example of the sounding curve. The phase over 90°, which is usually present in one of the off-diagonal components and at a lower frequency band, is sometimes referred to as an "anomalous" phase, because the data cannot be explained by 1-D or 2-D structure with isotropic resistivity media. The Kirishima case is especially unusual in that approximately half of the data show

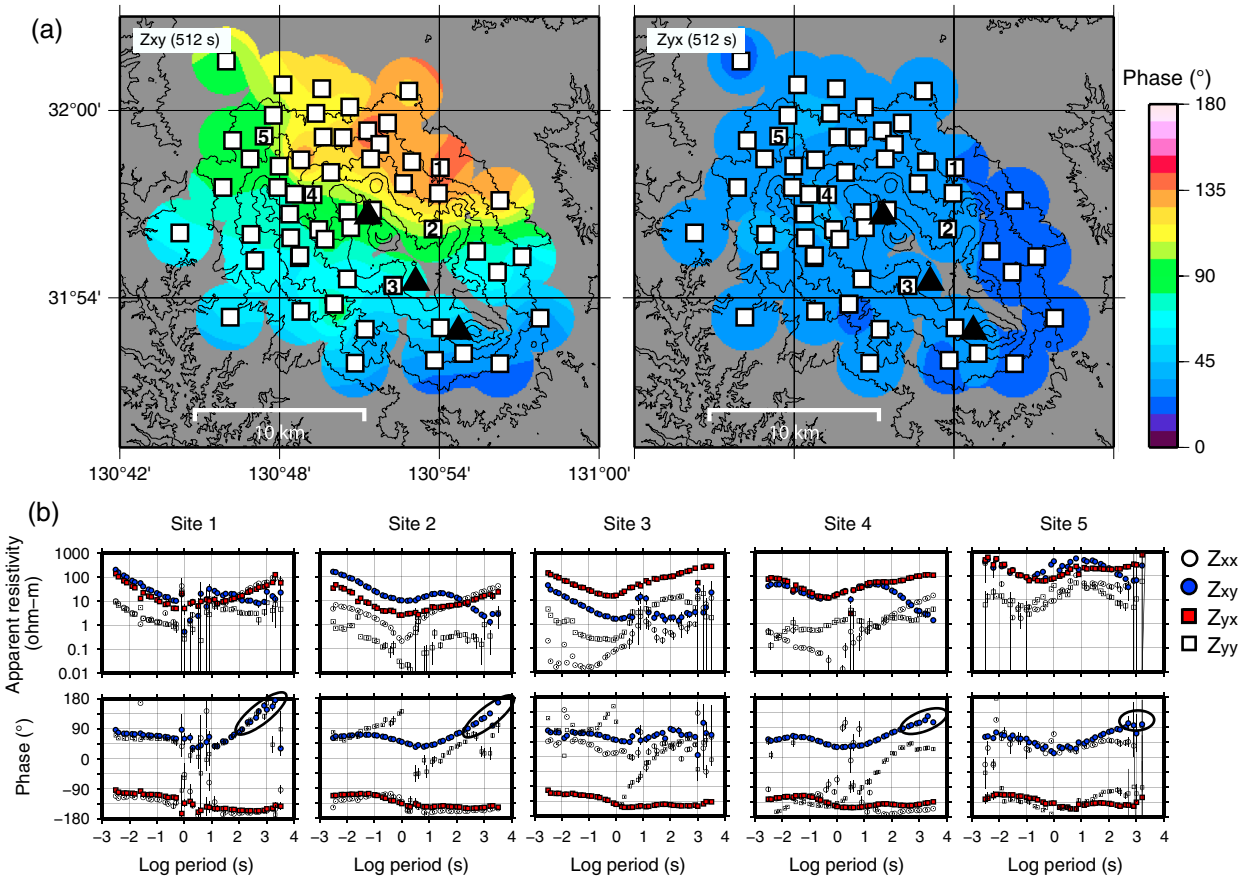

Figure 3. (a) Phase map of the Kirishima Volcanoes for the period of 512 s. To enable comparison between Z_{xy} and Z_{yx}, 180° is added to the phase of Z_{yx}. Open squares indicate the measurement sites, with sites numbered 1–5 indicating the locations of the sounding curves shown in Figures 3b, 9, and 13. The three solid triangles indicate, from northwest to southeast, the volcanoes of Iwo-yama, Shinmoe-dake, and Ohachi. (b) Examples of sounding curves for five sites. The anomalous phase that exceeds 90° is marked by solid ellipse.

an anomalous phase. Note that MT data recorded at the ocean floor sometimes shows phases less than 0°, which can be modeled by 2-D structure including high-conductivity seawater above measurement sites [*Constable et al.*, 2009; *Worzewski et al.*, 2011].

There are two general explanations for an anomalous phase. One explanation assumes resistivity anisotropy. Numerical calculations show that an anomalous phase occurs in the case where one anisotropic layer is overlain by another local anisotropic body and the anisotropic strikes differ significantly [*Pek and Verner*, 1997; *Heise and Pous*, 2003]. An alternative explanation assumes electric current channeling by particular 3-D features of the resistivity structure [*Egbert*, 1990]. For example, an L-shaped conductor generates current channeling and produces an anomalous phase around the corner of the "L" [*Ichihara and Mogi*, 2009; *Ichihara et al.*, 2013]. The model also requires 3 ~ 4 orders of resistivity contrast between conductor and surroundings. In this study, we adopt this latter idea to explain the anomalous phase found here, because there is no geological evidence that suggests the presence of two overlain anisotropic layers beneath the northern sector of the Kirishima Volcanoes.

5. 3-D Modeling

5.1. 3-D Inversion

It is usually difficult to explain an anomalous phase in real data, and previous studies have applied the forward approach rather than inversion [*Pous et al.*, 2002; *Lezaeta and Haak*, 2003]. However, here we try to explain the anomalous phase using an inversion because volcanic structures are usually too complex to be modeled using the forward approach.

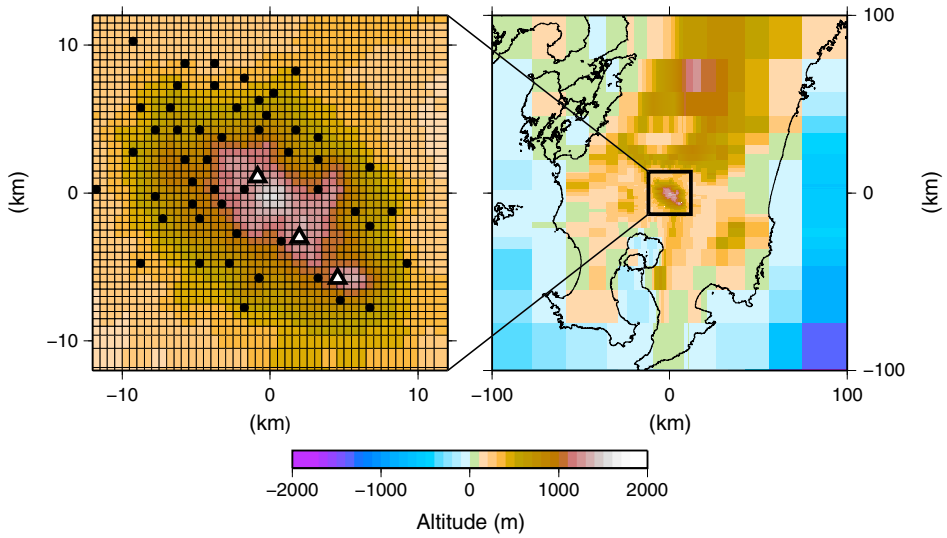

Figure 4. Mesh used in the inversion. The solid circles show the 53 MT measurement sites used in the inversion.

We inverted the MT response functions by using a 3-D code (WSINV3DMT) with an algorithm that transforms the model renewal equation from model space to data space [*Siripunvaraporn and Egbert*, 2000; *Siripunvaraporn et al*., 2005]. We used the latest version of WSINV3DMT [*Siripunvaraporn and Egbert*, 2009] in which the full impedance tensor (four complex components: Z_{xx}, Z_{xy}, Z_{yx}, and Z_{yy}) and geomagnetic transfer functions (two complex components: T_x and T_y) provided the inputs for the 3-D inversion. Fifty-three MT sites with good data quality were chosen, and the MT response functions in 16 periods (0.004, 0.008, 0.015, 0.05, 0.125, 0.4, 1, 3.2, 8, 25.6, 64, 128, 256, 512, 1024, and 2048 s) were used in the inversion. Therefore, basically there are 12 impedance/induction vector elements at 16 periods at each of the 53 sites.

The horizontal mesh size was set to 500 m in the area around the observation sites and was logarithmically increased with increasing distance from the Kirishima Volcanoes. The model also takes into account topography (Figure 4). The vertical mesh size was set at 100 m from the highest point to 1 km beneath sea level (bsl), and the air was approximated by 10^8 Ωm blocks. Between 1 and 10 km bsl, we set the vertical mesh size at 200–500 m. For depths below 10 km bsl, the mesh size was increased with increasing depth. The total mesh consisted of $66 \times 71 \times 58$ units (with seven vertical air layers as the default setting) in the *x*, *y*, and *z* directions, respectively. The calculation area was $234 \times 202 \times 208$ km, in which the ocean and bathymetry were represented by 0.25 Ωm blocks. The initial resistivity of the land was set as 100 Ωm. In each iteration, we replaced the prior model [*Siripunvaraporn and Egbert*, 2000] by the smallest-misfit model of the previous iteration.

In the chosen mesh, the MT response functions in the higher-frequencies cannot be correctly calculated. For example, diagonal components of impedance tensor and geomagnetic transfer functions (Z_{xx}, Z_{yy}, T_x, and T_y) approach zero as the frequency increases, because the code calculated the MT response functions at the center of each mesh. In order to practically avoid such kind of numerical problems, we omitted the part of the diagonal components and geomagnetic transfer functions at periods of less than 1 s.

In an initial inversion procedure, we first removed the noisy data by visual inspection and then assumed constant 10% error bars for the impedance tensor and constant 20% error bars for the geomagnetic transfer functions. By using the smoothing parameter ($\tau = 10$ with $\delta x = \delta y = \delta z = 0.1$) in the model covariance matrix, the root-mean-square (RMS) misfit had reduced from 29.7 to 2.74 after 13 iterations, and an apparently feasible structure was produced. However, importantly, the calculated phase was distributed over 0–90° and failed to explain the anomalous phase at all sites. This result did not change when we applied other smoothing parameters τ, which is initially set in each inversion, in the model covariance matrix [*Siripunvaraporn and Egbert*, 2000]. Because the anomalous phase is observed at approximately half the sites, the resistivity structure is regarded as unrealistic.

To construct a resistivity structure that explains the anomalous phase, we conducted another inversion using the following two-step inversion procedure. First, the error bars of Z_{xy} for the periods over 0.4 s, in which an

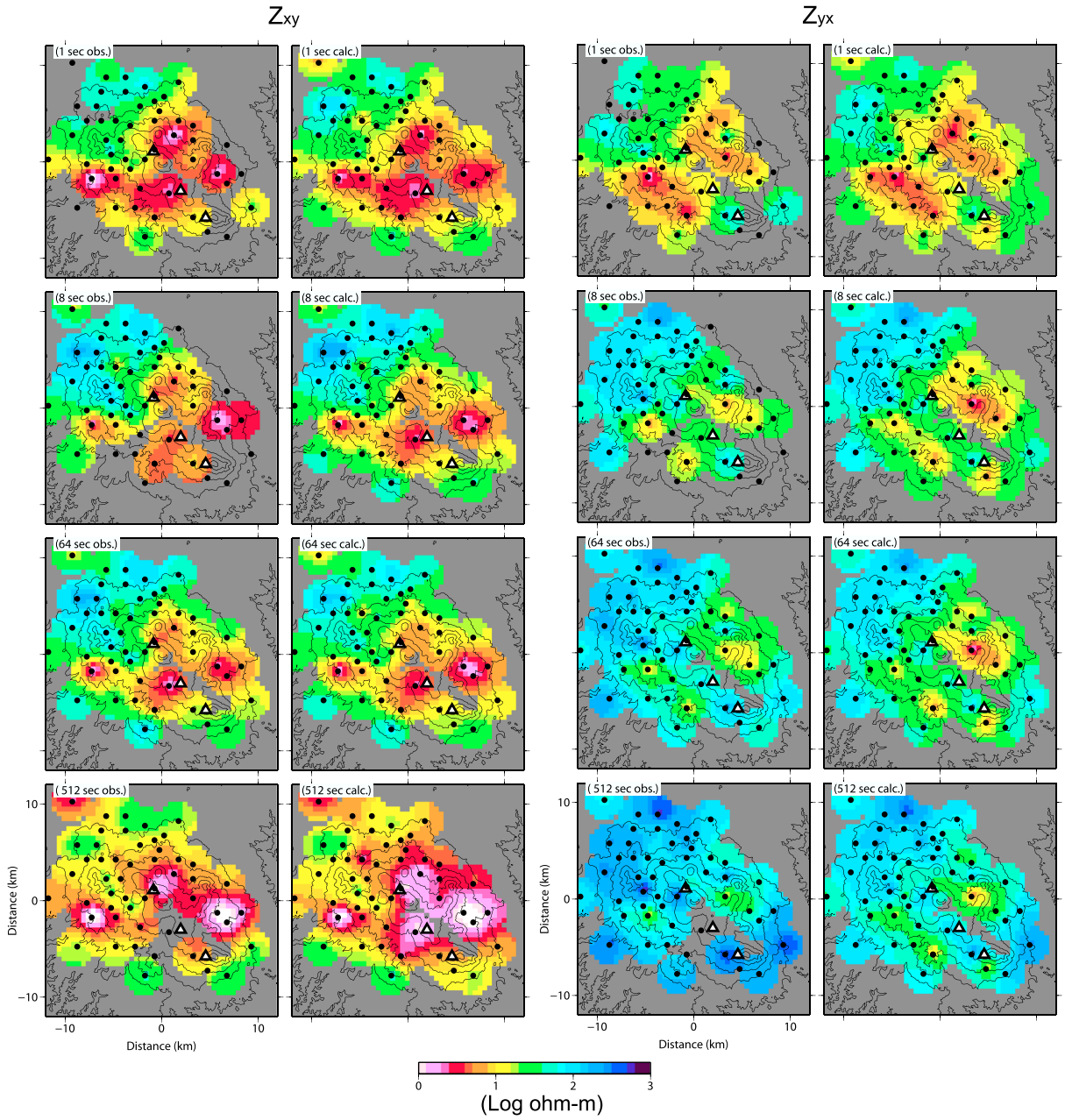

Figure 5. Apparent resistivity maps of the Kirishima Volcanoes for comparison of observed data ("obs.") with calculated response ("calc."). The off-diagonal components (Z_{xy} and Z_{yx}) of the impedance tensor are shown for representative periods of 1, 8, 64, and 512 s. The solid circles show the 53 MT measurement sites used in the inversion. Note that the noisy data are removed in the inversion. The three triangles indicate, from northwest to southeast, the volcanoes of Iwo-yama, Shinmoe-dake, and Ohachi (Figure 2).

anomalous phase is observed, were set to 2%. The other error bars were set at 10% for Z_{xx}, Z_{yx}, Z_{yy}, and 20% for the geomagnetic transfer functions. Using the uniform values of 100 Ωm for land and 0.25 Ωm for ocean, the inversion was conducted until the RMS misfit reached a stable level. Then, the error bars were recovered to the normal level (10% for Z and 20% for T), and the inversion was restarted by taking the final model of the first step as the prior and initial model for the next inversion. This two-step inversion was performed with three smoothing parameters ($\tau = 5$, 10, and 20 with $\delta x = \delta y = \delta z = 0.1$) in the model covariance matrix [*Siripunvaraporn and Egbert*, 2000]. The model with $\tau = 10$ was selected as the final model that produced a smallest RMS. Although the initial model (100 Ωm for land) produced a relatively large RMS value of 38.6 due to the small error bars on Z_{xy}, the two-step inversion produced a final RMS of 1.95 with 10% errors for Z and 20% errors for T, which is smaller than for the usual inversion (RMS = 2.74 with the same error bars).

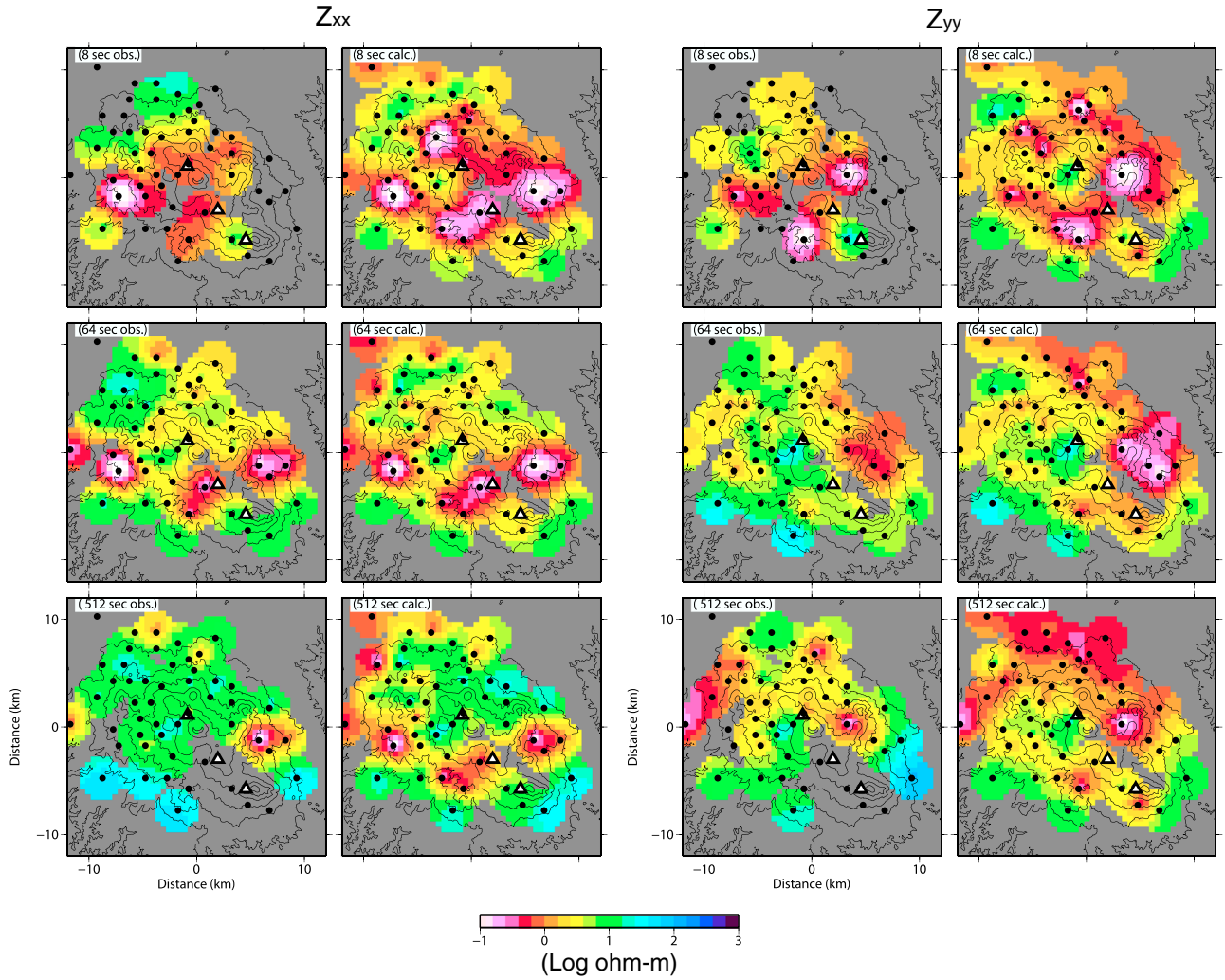

Figure 6. Apparent resistivity map for comparison of observed data (obs.) with calculated response (calc.). The diagonal components (Z_{xx} and Z_{yy}) of the impedance tensor are shown. Other notations are the same as in Figure 5.

Figures 5–8 compare the observed data with the response calculated from the final resistivity structure. For simplicity, the apparent resistivity and phase of the impedance tensor (Z_{xx}, Z_{xy}, Z_{yx}, and Z_{yy}) are shown for periods of 1, 8, 64, and 512 s. Note that the parts of the diagonal components (Z_{xx} and Z_{yy}) less than 1 s are not used in the inversion. Overall, the model explains the observed data. Figure 9 presents an example of the data fit shown by sounding curves. Although the fit is not perfect, the anomalous phase is successfully explained by the structure. This work (both of steps 1 and 2) is the first inversion study that explains the anomalous phase in real fields. The anomalous phase is relatively well explained in the first step of the inversion, whereas the better misfit is obtained in the second step and overall tendency of the data is well reproduced (Figure 9).

Figure 10 shows the data fit for the induction vectors [*Parkinson*, 1962] and phase tensor ellipses [*Caldwell et al.*, 2004; *Moorkamp*, 2007], which are robust to the galvanic distortion near the surface. It should be noted that we did not invert the phase tensors but did invert the impedance tensor. The calculated response provides a reasonable explanation of the overall data, but there is a notable difference in the phase tensor for 512 s. In the data, the determinant of the phase tensor (Φ_2) became negative at the northern sites where an anomalous phase is observed. In contrast, Φ_2 of the calculated phase tensor are positive except two sites. Note that negative Φ_2 are reproduced in nine sites in step 1. It should be noted here that the main features of the resistivity structure discussed in the following sections do not significantly differ between step 1 and step 2. Therefore, we conclude that the polarity of Φ_2 is not essential for the structure.

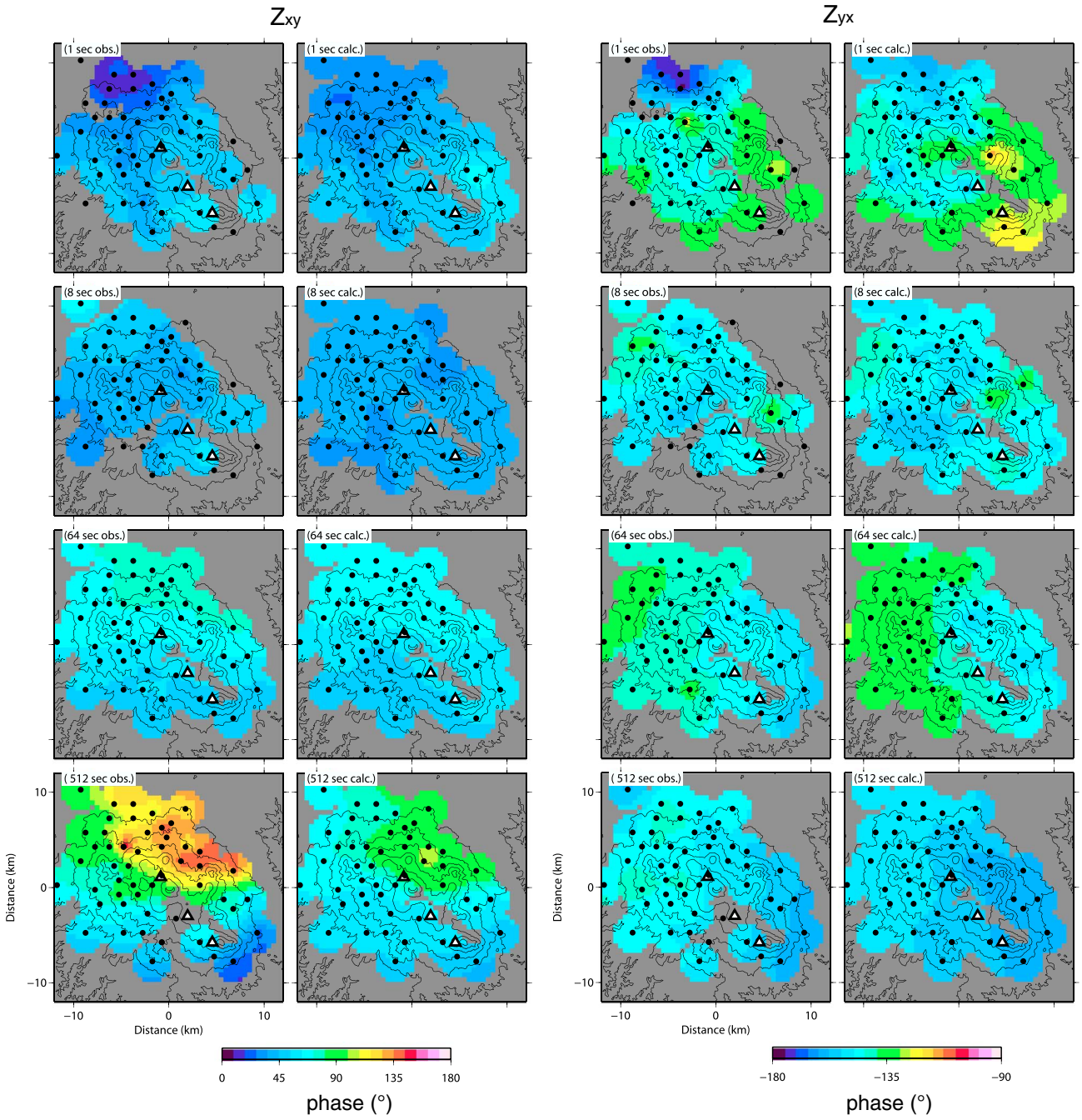

Figure 7. Phase map of the Kirishima Volcanoes for comparison of observed data (obs.) with calculated response (calc.). The off-diagonal components (Z_{xy} and Z_{yx}) of the impedance tensor are shown. Other notations are the same as in Figure 5.

5.2. 3-D Resistivity Structure

Figures 11 and 12 show the horizontal and vertical slices of the final resistivity structure, respectively. Horizontal slices (Figure 11) show that a widespread conductor in the shallower part gradually localizes with increasing depth. In particular, the conductor is localized NE of Iwo-yama at 6 km bsl. The subvertical conductor is clearly seen in the vertical slices (labeled C1 in Figures 11, 12). At shallow depths, the vertical conductor becomes obscure and is replaced by the pervasive conductive layers. Figures 11, 12 also show a large conductive body (labeled C2) exists northwest of the Shinmoe-dake. The vertical slices (Figure 12) show

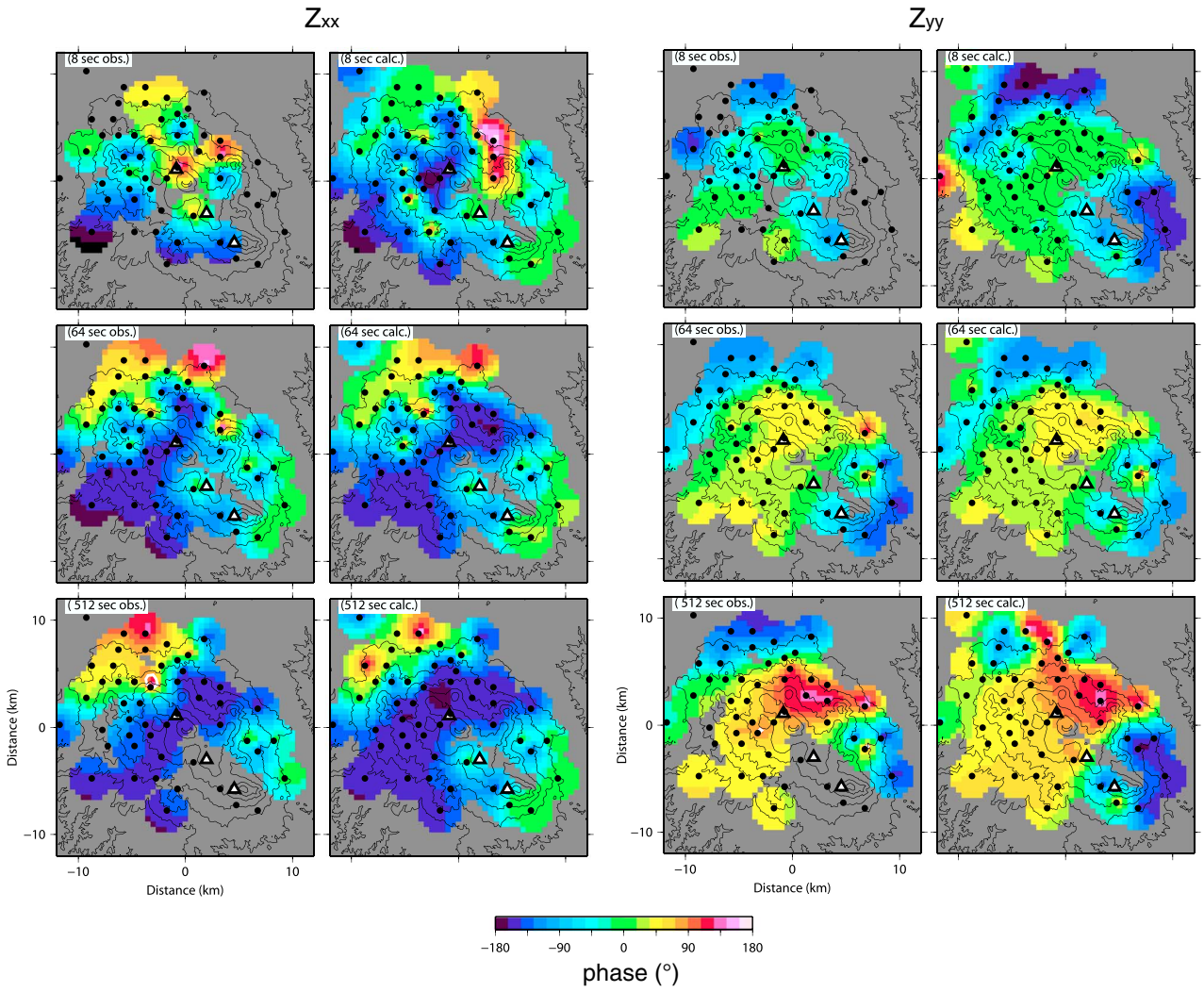

Figure 8. Phase map of the Kirishima Volcanoes for comparison of observed data (obs.) with calculated response (calc.). The diagonal components (Z_{xx} and Z_{yy}) of the impedance tensor are shown. Other notations are the same as in Figure 5.

that the top of the deep conductor corresponds approximately to 10 km bsl. Although the entire shape of the deep conductor is not clear due to its extension to the west, away from the site coverage, its volume is estimated to be in excess of 100 km^3. The subvertical conductor (C1) is located between shallow conductive layer and the deep conductive body (C2).

The resistivity structure shows a high contrast in the resistivity value. In particular, at 3 km bsl, this contrast reaches up to 5 orders of magnitude. The Kakuto caldera corresponds to the resistive zone (*R*1 in Figures 11, 12). At 3 km bsl, there is another resistive zone that lies just above the 2011 deformation source (*R*2 in Figures 11, 12). At present, it is unclear whether this resistive zone (R2) is related to the Kakuto caldera, because the activity of the Kirishima Volcanoes destroyed and covered the southern rim of the caldera.

It should be noted that the features of the 3-D structure (high resistivity contrast, subvertical conductor, and deep conductive body) are not present in the models that fail to explain the anomalous phase. The relationship between the anomalous phase and 3-D subsurface structure is discussed in section 5.3.

5.3. Verification of the Main Features of the Structure

The fit between the data and the calculated response (Figures 5–10) is not perfect, and therefore, there is a possibility that the structural features are not unique for the same level of fit to the observations. Therefore, the robustness of the structural features identified needs to be carefully checked.

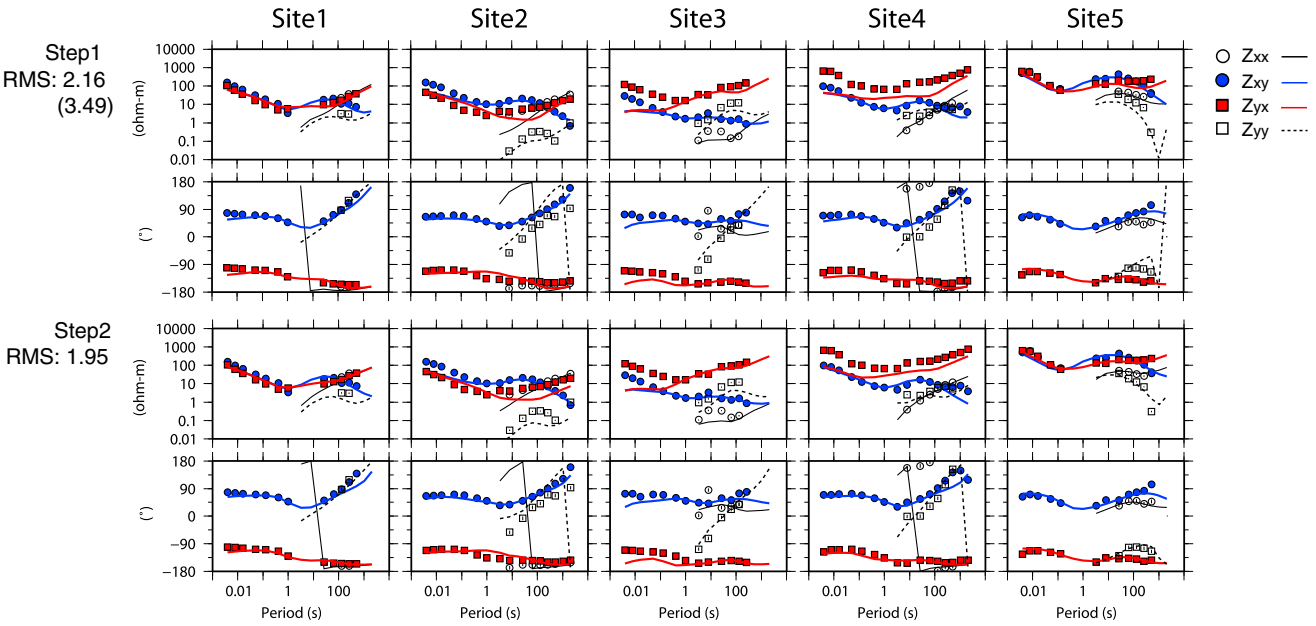

Figure 9. Representative sounding curves for comparison of observed data (symbols) with calculated response (lines). Error bars given in the inversion are smaller than each symbol. The locations of the sites are shown in Figure 4. The data show the 16 periods used in the inversion. Note that the parts of the diagonal components (Z_{xx} and Z_{yy}) less than 1 s were not used in the inversion. The inversion was conducted in two steps as detailed in section 5.1. The RMS misfits of 3.49 and 2.16 shown in step 1 were calculated by using the error bars used in step 1 and step 2, respectively (both RMS are calculated from the final model of step 1).

To check the presence of the conductors, two sensitivity tests were performed. First, the resistivities less than 100 Ωm in the zone of $-1000\,\text{m} < x < 5000\,\text{m}$, $-3000\,\text{m} < y < 5000\,\text{m}$, and at 2–10 km bsl were all changed to 100 Ωm. This elimination of the subvertical conductor (C1) resulted in an increase of the RMS misfit from 1.95 to 2.19, and the corresponding changes in the sounding curves are presented in Figure 13b. The sensitivity test was also applied to the zone around the deep conductor, which is defined as the conductive zone (less than 100 Ωm) at $-7000\,\text{m} < x < 9000\,\text{m}$, $-15{,}000 < y < 0$, and at 10–20 km bsl. This elimination of the deep conductor (C2) resulted in an increase of the RMS misfit from 1.95 to 2.15. The corresponding changes in the sounding curves are shown in Figure 13c. The sensitivity tests validated that both the subvertical conductors and deep conductors are necessary for the data. In particular, Figure 13 shows that the anomalous phase is essential for the structure.

6. Discussion

A subvertical conductor at a depth of 2–10 km is the most prominent feature of the resistivity structure. Figures 11 and 12 show that the conductor corresponds to the zone of low seismicity. Assuming a low strain rate (10^{-14}/s), the lower bound of earthquakes (brittle–plastic transition) corresponds approximately to the 370–400°C isotherm [*Fournier*, 1999]. A higher strain rate would make it possible for earthquakes to occur in a higher-temperature regime. Given that the higher strain rate is plausible in a volcanic area, we suggest that the temperature in the vertical conductor is over 400°C. A subvertical conductor at upper crustal levels has recently been imaged at other volcanoes: Ruapehu, New Zealand [*Ingham et al*., 2009]; St. Helens, U.S. [*Hill et al*., 2009]; and the southeastern part of the Taupo volcanic zone, New Zealand [*Bertrand et al*., 2012]. However, the interpretations in those studies are quite different from each other. For example, *Hill et al*. [2009] suggested partial melt, whereas *Bertrand et al*. [2012] suggested hydrothermal fluid as a cause of high conductivity. Because both melt and hydrothermal aqueous fluids can be conductive at 0.1 Ωm [*Nesbitt*, 1993; *Gaillard et al*., 2008; *Ni et al*., 2011], it is impossible to interpret the nature of the conductor solely from the resistivity value.

Figure 11 shows that the zone between the deformation source and the Shinmoe crater is resistive, whereas the northern part of the Shinmoe crater is significantly conductive. In this study, we assume that magma tends to travel through a conductor rather than a zone of high resistivity, because low resistivity suggests a

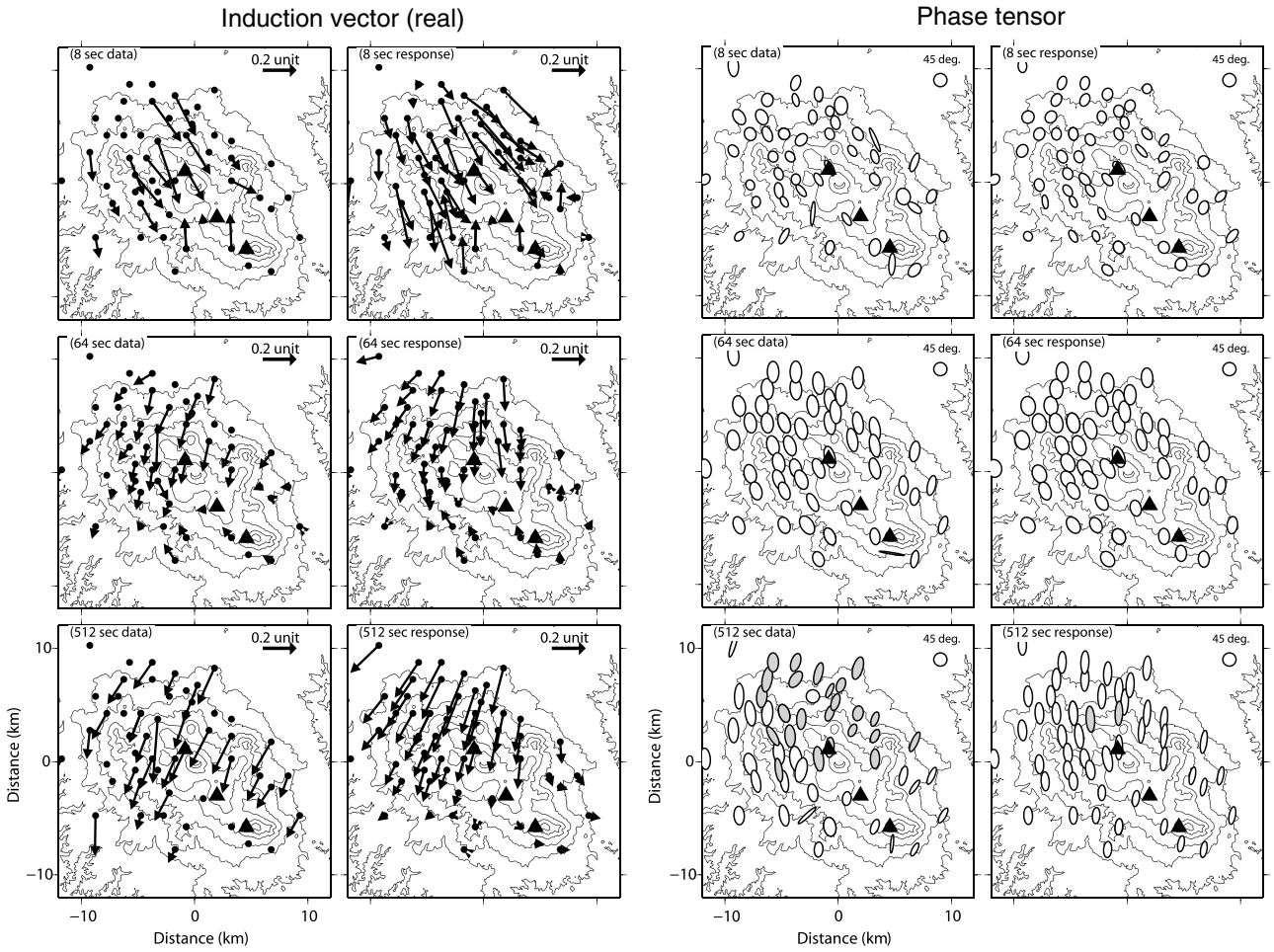

Figure 10. (left) Induction (Parkinson criteria) vectors and (right) phase tensor ellipse for the comparison of observed data with calculated response. In this study, axes of phase tensor ellipse (Φ_{max} and Φ_{min}) are calculated according to the slightly modified expression [*Moorkamp*, 2007]. At a site where Φ_{min} is negative, phase tensor ellipses are represented by using $|\Phi_{min}|$ and are filled with grey color. Note that the noisy data were not used in the inversion.

good network of pore fluids. Considering that precursory earthquakes were not observed in 2011 between the deformation source and the Shinmoe crater, it is unlikely that the magma traveled straight to the crater through the resistive zone. On the basis of the spatial relationship between the conductor and the source of syn-eruptive subsidence (Figures 11 and 12), we propose that the subvertical conductor acted as a magma pathway for the 2011 eruptions, which extends from the deformation source to the Shinmoe crater via the northern part of the Shinmoe Volcano. Two observations support the hypothesis that the magma was derived from the northern part of the Shinmoe crater. The first is the seismicity beneath the Shinmoe Volcano. Line FF' in Figure 12 shows that the hypocenter of the seismicity became shallower from north to the Shinmoe crater. The second observation is that shallow seismic tremors occurred during the 2011 eruptions. Based on continuous long-term seismic array observations, it is suggested that the volcanic tremors occurred at 1 km depth and 1 km from the northern part of the Shinmoe crater [*Nakamichi et al.*, 2013].

Although the subvertical conductor is interpreted as a magma pathway, we consider that the volume of magma is far too small compared with the volume of the aqueous hydrothermal fluids. Taking into account that the subvertical conductor is significantly larger than the volume of magma erupted in 2011 (0.021–0.027 km^3), it is unreasonable to assume that the interconnected melt is present everywhere in the subvertical conductor. A previous study also rejected the presence of a large amount of melt at the depth of the subvertical conductor [*Yamamoto and Ida*, 1997]. In this study, we interpret the vertical conductor as a volcanic conduit through which hot volcanic fluids and, potentially, magma are transported to craters [*Ingham et al.*, 2009]. The vertical

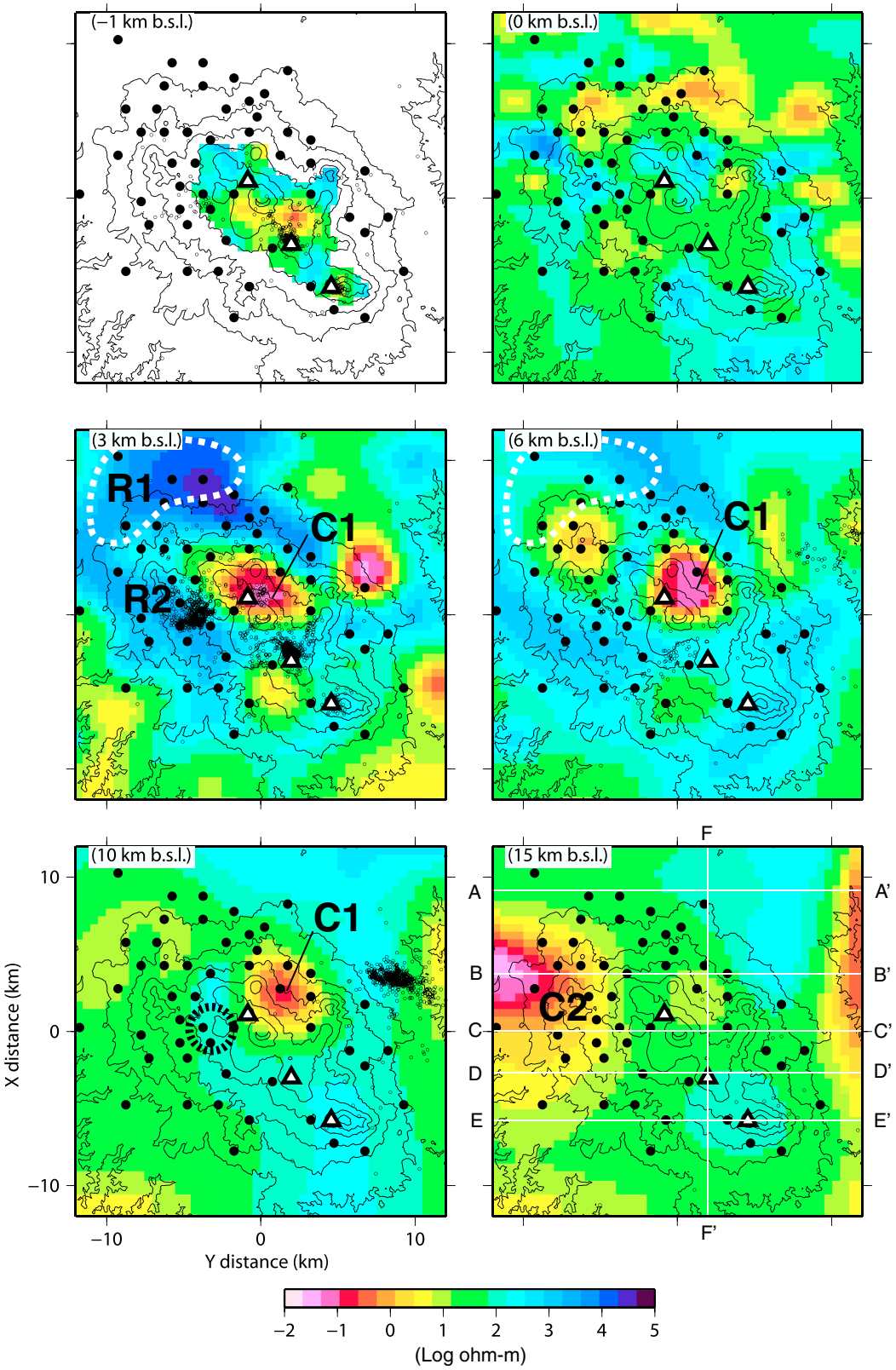

Figure 11. Horizontal slices of the final resistivity structure at various depths. The air above sea level was approximated by 10^8 Ωm resistivity blocks. The seismicity between March 2008 and June 2012 (J. Oikawa, personal communication, 2013) is shown by small circles. Lines A–A′ to F–F′ indicate transects along which vertical slices were taken as displayed in Figure 12. C1 and C2 indicate the subvertical conductor and the deep conductor, respectively. R1 and R2 indicate the resistive zone beneath the Kakuto caldera and the resistive zone above the 2011 deformation source, respectively. Other notations are the same as in Figure 5. The region enclosed by the white dashed line shows the hypocentral location of the 1968–1969 Ebino earthquake swarm [*Minakami et al.*, 1969].

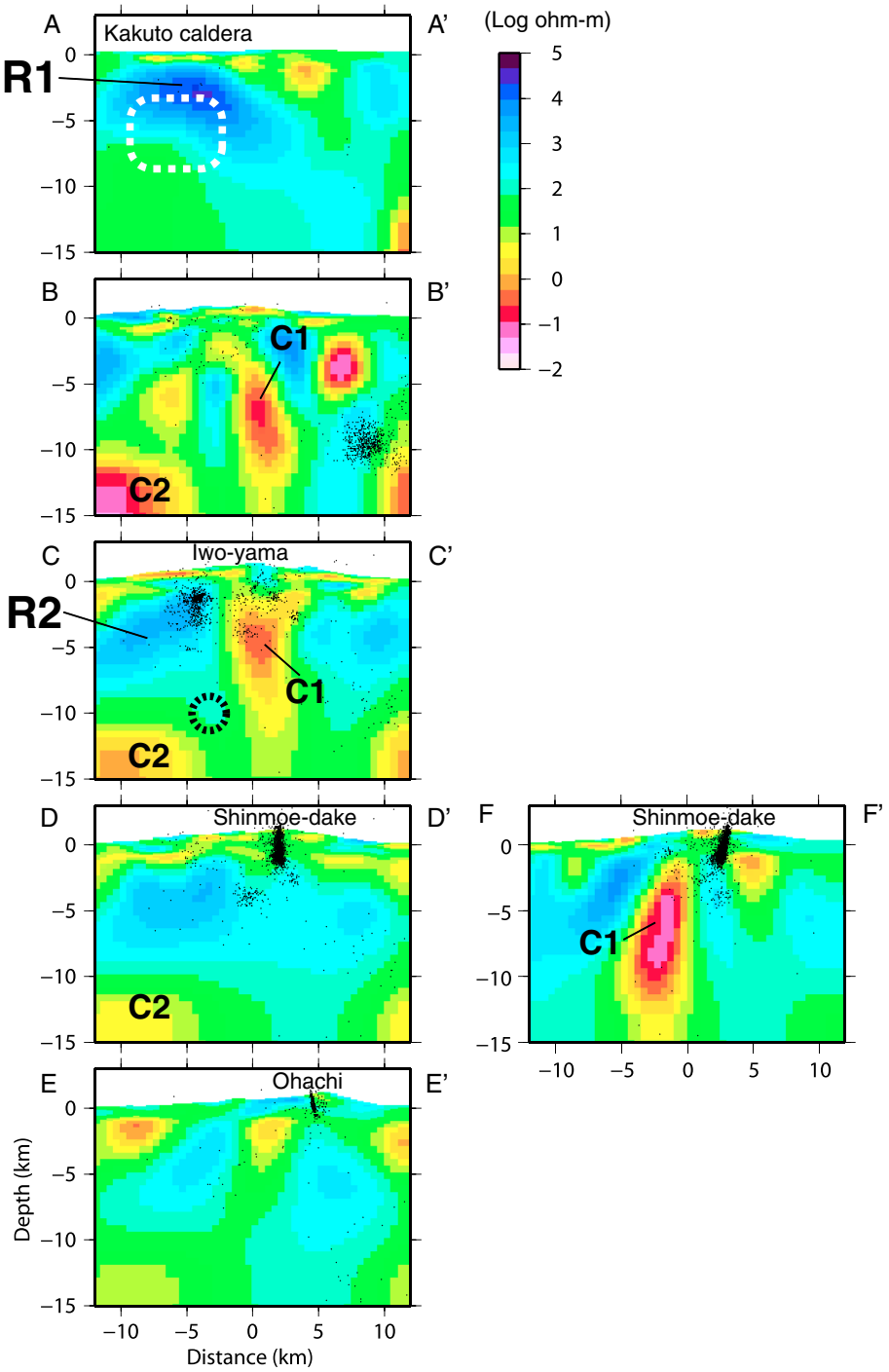

Figure 12. Vertical slices of the final resistivity structure W–E (transects A–A′ to E–E′ in Figure 11) and N–S (transect F–F′ in Figure 11) across the study area. The seismicity between March 2008 and June 2012 (J. Oikawa, personal communication, 2013) is shown as a 2 km wide swath. The white dashed region along A–A′ shows the hypocentral location of the 1968–1969 Ebino earthquake swarm [*Minakami et al.*, 1969]. The black dashed circle indicates the possible location of the source of deformation [*Ueda et al.*, 2013; *Nakao et al.*, 2013; *Kozono et al.*, 2013].

conductor extends upward to the volcanic cones (Iwo-yama and Shinmoe-dake) in the central sector of the Kirishima volcano group, whereas it is directed away from the SW volcanic cone area (Ohachi). This result is broadly consistent with the findings from 1-D inversion of previous ULF–MT data [*Utada et al.*, 1994; *Kagiyama et al.*, 1997].

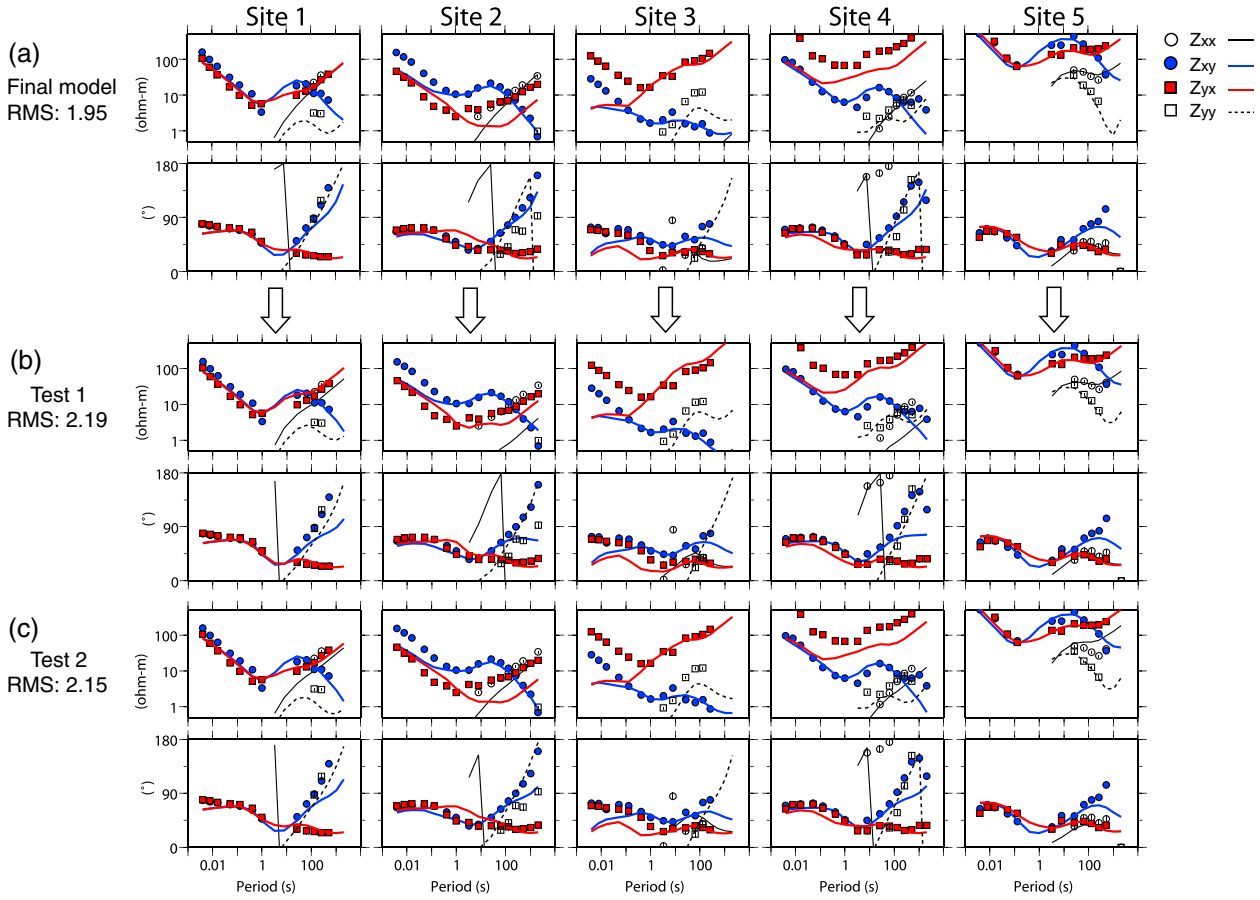

Figure 13. Results of sensitivity tests. Notations are the same as in Figure 9. (a) Sounding curve calculated from the final resistivity structure. (b) Result of sensitivity test that eliminates the subvertical conductor. (c) Result of sensitivity test that eliminates the deep conductor.

Hydrothermally altered minerals (especially smectite) show a significantly low resistivity, and this has been considered an important cause of the low resistivity within active volcanoes [e.g., *Jones and Dumas*, 1993; *Ogawa et al*., 1998; *Nurhasan et al*., 2006; *Coppo et al*., 2008; *Aizawa et al*., 2009a; *Yamaya et al*., 2009; *Garcia and Jones*, 2010; *Kanda et al*., 2010; *Siniscalchi et al*., 2012]. By taking into account bore data at Ogiri geothermal field [*Uchida and Sasaki*, 2006], the widespread, shallow (a few kilometers deep) conductors are interpreted as a zone of hydrothermal alteration whose base corresponds to the 200°C isotherm. Conversely, the alteration in the subvertical conductor is difficult to evaluate because smectite breaks down at temperatures above 200°C. Little is known about hydrothermal alteration and its electrical resistivity at temperatures over 400°C.

Petrological data give important insights into the magma plumbing system of the Shinmoe-dake Volcano. *Suzuki et al*. [2013] showed that the erupted material of the 2011 eruptions comprises a mixture of basaltic andesite (BA) and silicic andesite (SA) and suggested that magma mixing occurred in two stages (precursor mixing followed by final mixing) before the sub-Plinian eruptions. The timescale from the final mixing to the eruption was estimated at 2–50 h. According to melt inclusion analysis and phase equilibria experiments [*Suzuki et al*., 2013], the reservoir of SA magma was located at a depth of 5 km, whereas BA magma was supplied from a deeper level (>10 km). Because the subvertical conductor exists on its own at around 5 km depth, the SA magma is interpreted to be contained in the subvertical conductor. In turn, the BA magma is interpreted as occupying the deep conductor (C2) below 10 km. The location of the deep conductor is roughly consistent with the locations of the deep low-velocity zone [*Yamamoto and Ida*, 1994] and the deep low-attenuation zone [*Yamamoto and Ida*, 1997], and a large BA magma chamber may exist there. Here it should be noted that the 2011 deformation source is located above the eastern and upper rim of the deep

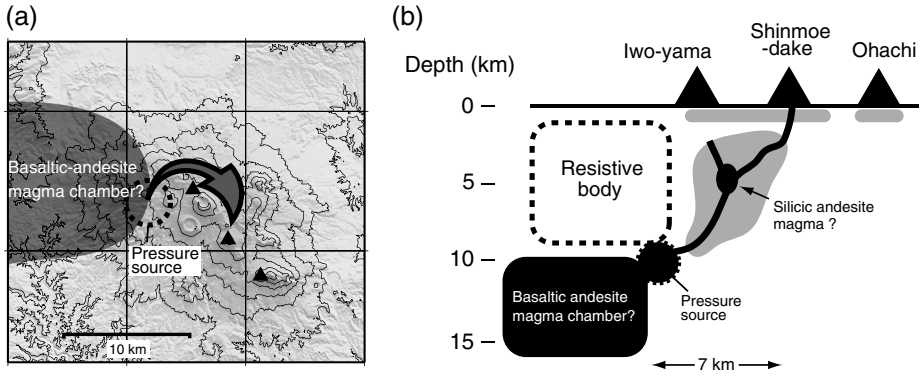

Figure 14. Schematic illustration of the magma plumbing system of Shinmoe-dake Volcano. The model is inferred from the 3-D resistivity structure (Figures 11 and 12) and studies of the 2011 sub-Plinian eruptions at Shinmoe-dake. (a) Horizontal view of the magma movement. The dark shaded area indicates the chamber of the basaltic andesite (BA) magma. The dashed circle indicates the magma intrusion zone that corresponds to the location of the syn-eruptive deformation source [*Ueda et al*., 2013; *Nakao et al*., 2013; *Kozono et al*., 2013]. The arrow indicates the inferred magma movement of the 2011 Shinmoe-dake eruptions. (b) Vertical view of the magma movement in the 2011 Shinmoe-dake eruptions (corresponding to the arrow in Figure 14a). The black area represents the zone of interconnected melt, whereas the grey area indicates the zone of aqueous fluid. Both the black and grey areas are imaged as low-resistivity regions.

conductor (Figures 11 and 12). Therefore, the preeruptive and posteruptive inflations are interpreted as the intrusion of BA magma from the deep chamber. In turn, the syn-eruption deflation is interpreted as corresponding to the evacuation of magma through the identified magma pathway.

The spatial relationship between the syn-eruptive subsidence and the Shinmoe-dake crater (Figures 2 and 11) indicates that the magma traveled obliquely to the surface. The highly resistive body is located just above the deformation source (Figures 11 and 12) and possible BA magma chamber. We speculate that this highly resistive body impeded the ascent of magma during the 2011 eruptions. Similar structural controls on subsurface magmatic fluid movement have been suggested for Asama and Iwate Volcanoes in Japan [*Aizawa et al*., 2008, 2009b]. Figure 14 shows a schematic image of the magma plumbing system of the Kirishima Volcanoes. The deep conductive body is the magma chamber from which BA magma was supplied to the volcanoes (e.g., Iwo-yama and Shinmoe-dake Volcanoes) in the central sector of the Kirishima volcano group. From February 2010 to January 2011, BA magma continuously intruded into the zone above the deep chamber. Prior to the 2011 eruptions, the interconnected melt pathway was formed somewhere in the subvertical conductor. From the shape of the subvertical conductor, it is inferred that the erupted magma in 2011 moved from the NW via the northern part of Shinmoe-dake Volcano (Figure 14a).

The Kakuto caldera (Figures 1 and 2) was imaged as being of high resistivity, especially to a depth of 5 km bsl. This result is consistent with a previous 2-D inversion [*Goto et al*., 1997]. Because the high resistivity (3000–10,000 Ωm) is inconsistent with the presence of an interconnected melt, there is unlikely to be an accumulation of a large mass of magma beneath the Kakuto caldera. Alternatively, the resistive body may represent a fossilized magma chamber, which has cooled and solidified. The hypocentral area of the 1968–1969 earthquakes corresponds to the deeper part of the resistive body (Figures 11 and 12), which is consistent with the conclusion of *Goto et al*. [1997] that a large mass of fluid is unlikely to exist in the hypocentral area. However, because the conductor is located at the southeastern rim and bottom of the hypocentral area (Figures 11 and 12), we further suggest that earthquakes beneath Kakuto caldera are related to volcanic fluids. The intermittent earthquake swarms may be caused by pressure increase around the conductor or the partial migration of volcanic fluid.

7. Conclusions

The 3-D resistivity structure in the vicinity of Shinmoe-dake Volcano reveals a subvertical conductor that is located between the deep-seated conductive body (at a depth greater than 10 km) and shallow conductive layers. By applying the findings of geophysical and petrological studies of the 2011 sub-Plinian eruptions at Shinmoe-dake Volcano, and assuming that magma travels through a conductor rather than through a zone of high resistivity, we propose that the subvertical conductor represents the hydrothermal zone at temperatures

over 400°C, in which a magma pathway (interconnected melt) is partially and occasionally formed before magmatic eruptions. Subvertical conductors in the upper crust have recently been found under other active volcanoes. We consider that the precise imaging of the subvertical conductor and comparing it with other observations (seismicity, deformation, and erupted material) is the key to investigating magma plumbing systems under active volcanoes.

Acknowledgments

Existing MT data were kindly provided by T. Goto (Kyoto University), T. Uchida (Geological Survey of Japan, AIST), New Energy and Industrial Technology Development Organization, and Nittetsu Kagoshima Geothermal Co., Ltd. The geomagnetic data used for the remote reference processing were provided by the Kakioka Geomagnetic Observatory, Japan Meteorological Agency. We thank landowners and regional forest offices (Kagoshima and Miyazaki prefectures) for permitting the observations to be conducted. F. Masutani, M. Yamaguchi, T. Kagiyama, Y. Sasai, and H. Utada contributed to acquiring the previous MT data in the region of the Ebino earthquake swarms. Y. Maehara and T. Sugano are thanked for their participation in the field campaign of 2010. The MT observations in 2011 were conducted under the supervision of the Japan Meteorological Agency. Hypocenter data were kindly provided by J. Oikawa (ERI: Earthquake Research Institute, University of Tokyo). For this study, We have used the computer systems of the Earthquake Information Center of the Earthquake Research Institute, the University of Tokyo. We thank W. Siripunvaraporn for supplying his 3-D inversion code. We thank A. Chave for providing his magnetotelluric analysis program. A discussion with H. Ichihara (JAMSTEC) about the anomalous phase was helpful for the 3-D modeling. We thank ERI for permitting the use of a published figure (Figure 1). The comments from Malcolm Ingham and an anonymous reviewer and the associated editor (Max Moorkamp) greatly improved the manuscript. This work was supported by a grant-in-aid from MEXT (KAKENHI 22900001 and the HIZUMI project).

References

Aizawa, K., Y. Ogawa, T. Hashimoto, T. Koyama, W. Kanda, Y. Yamaya, M. Mishina, and T. Kagiyama (2008), Shallow resistivity structure of Asama Volcano and its implications for magma ascent process in the 2004 eruption, *J. Volcanol. Geotherm. Res.*, *173*, 165–177, doi:10.1016/j.jvolgeores.2008.01.016.

Aizawa, K., Y. Ogawa, and T. Ishido (2009a), Groundwater flow and hydrothermal systems within volcanic edifices: Delineation by electric self-potential and magnetotellurics, *J. Geophys. Res.*, *114*, B01208, doi:10.1029/2008JB005910.

Aizawa, K., Y. Ogawa, M. Mishina, K. Takahashi, S. Nagaoka, N. Takagi, S. Sakanaka, and T. Miura (2009b), Structural controls on the 1998 volcanic unrest at Iwate volcano: Relationship between a shallow, electrically resistive body and the possible ascent route of magmatic fluid, *J. Volcanol. Geotherm. Res.*, *187*, 131–139, doi:10.1016/j.jvolgeores.2009.08.009.

Aizawa, K., T. Koyama, M. Uyeshima, H. Hase, T. Hashimoto, W. Kanda, R. Yoshimura, M. Utsugi, Y. Ogawa, and K. Yamazaki (2013), Magnetotelluric and temperature monitoring after the 2011 sub-Plinian eruptions of Shinmoe-dake volcano, *Earth Planets Space*, 539–550.

Bertrand, E. A., et al. (2012), Magnetotelluric imaging of upper-crustal convection plumes beneath the Taupo Volcanic Zone, New Zealand, *Geophys. Res. Lett.*, *39*, L02304, doi:10.1029/2011GL050177.

Caldwell, T. G., H. M. Bibby, and C. Brown (2004), The magnetotelluric phase tensor, *Geophys. J. Int.*, *158*, doi:10.1111/j.1365-246X.2004.02281.x.

Chave, A. D., and D. J. Thomson (2004), Bounded influence magnetotelluric response function estimation, *Geophys. J. Int.*, *157*, 988–1006, doi:10.1111/j.1365-246X.2004.02203.x.

Constable, S., K. Key, and L. Lewis (2009), Mapping offshore sedimentary structure using electromagnetic methods and terrain effects in marine magnetotelluric data, *Geophys. J. Int.*, *176*, 431–442, doi:10.1111/j.1365-246X.2008.03975.x.

Coppo, N., P. A. Schnegg, W. Heise, P. Falco, and R. Costa (2008), Multiple caldera collapses inferred from the shallow electrical resistivity signature of the Las Cañadas caldera, Tenerife, Canary Islands, *J. Volcanol. Geotherm. Res.*, *170*, 153–166, doi:10.1016/j.jvolgeores.2007.09.013.

Egbert, G. D. (1990), Concerning dispersion-relations for the magnetotelluric impedance tensor—Comment, *Geophys. J. Int.*, *102*, 1–8, doi:10.1111/j.1365-246X.1990.tb00525.x.

Fournier, R. O. (1999), Hydrothermal processes related to movement of fluid from plastic into brittle rock in the magmatic-epithermal environment, *Econ. Geol. Bull. Soc. Econ. Geol.*, *94*, 1193–1211.

Gaillard, F., and G. I. Marziano (2005), Electrical conductivity of magma in the course of crystallization controlled by their residual liquid composition, *J. Geophys. Res.*, *110*, B06204, doi:10.1029/2004JB003282.

Gaillard, F., M. Malki, G. Iacono-Marziano, M. Pichavant, and B. Scaillet (2008), Carbonatite melts and electrical conductivity in the asthenosphere, *Science*, *322*, 1363–1365, doi:10.1126/science.1164446.

Gamble, T. D., J. Clarke, and W. M. Goubau (1979), Magnetotellurics with a remote magnetic reference, *Geophysics*, *44*, 53–68.

Garcia, X., and A. G. Jones (2010), Internal structure of the western flank of the Cumbre Vieja volcano, La Palma, Canary Islands, from land magnetotelluric imaging, *J. Geophys. Res.*, *115*, B07104, doi:10.1029/2009JB006445.

Goto, T., N. Oshiman, and N. Sumitomo (1997), The resistivity structure around the hypocentral area of the Ebino earthquake swarm in Kyushu district, Japan, *J. Geomagn. Geoelectr.*, *49*, 1279–1291.

Heise, W., and J. Pous (2003), Anomalous phases exceeding 90 degrees in magnetotellurics: Anisotropic model studies and a field example, *Geophys. J. Int.*, *155*, 308–318.

Heise, W., T. G. Caldwell, H. M. Bibby, and S. L. Bennie (2010), Three-dimensional electrical resistivity image of magma beneath an active continental rift, Taupo Volcanic Zone, New Zealand, *Geophys. Res. Lett.*, *37*, L10301, doi:10.1029/2010GL043110.

Hill, G. J., T. G. Caldwell, W. Heise, D. G. Chertkoff, H. M. Bibby, M. K. Burgess, J. P. Cull, and R. A. F. Cas (2009), Distribution of melt beneath Mount St Helens and Mount Adams inferred from magnetotelluric data, *Nat. Geosci.*, *2*, 785–789, doi:10.1038/ngeo661.

Ichihara, H., and T. Mogi (2009), A realistic 3-D resistivity model explaining anomalous large magnetotelluric phases: The L-shaped conductor model, *Geophys. J. Int.*, *179*, 14–17, doi:10.1111/j.1365-246X.2009.04310.x.

Ichihara, H., T. Mogi, and Y. Yamaya (2013), Three-dimensional resistivity modelling of a seismogenic area in an oblique subduction zone in the western Kurile arc: Constraints from anomalous magnetotelluric phases, *Tectonophysics*, *603*, 114–122, doi:10.1016/j.tecto.2013.05.020.

Ida, Y., M. Yamaguchi, and F. Masutani (1986), Recent seismicity and stress field in Kirishima volcano, *Bull. Earthquake Res. Inst. Univ. Tokyo*, *39*, 111–121.

Imura, R. (1994), Geology of Kirhishima volcano, *Bull. Earthquake Res. Inst. Univ. Tokyo*, *69*, 189–209.

Imura, R., and T. Kobayashi (1991), Eruptions of Shinmoedake Volcano, Kirishima volcano group, in the last 300 years, *Bull. Volcanol. Soc. Jpn.* (in Japanese with English abstract), *36*, 135–148.

Ingham, M. R., H. M. Bibby, W. Heise, K. A. Jones, P. Cairns, S. Dravitzki, S. L. Bennie, T. G. Caldwell, and Y. Ogawa (2009), A magnetotelluric study of Mount Ruapehu volcano, New Zealand, *Geophys. J. Int.*, *179*, 887–904, doi:10.1111/j.1365-246X.2009.04317.x.

Jones, A. G., and I. Dumas (1993), Electromagnetic images of a volcanic zone, *Phys. Earth Planet. Inter.*, *81*, 289–314.

Kagiyama, T., H. Utada, H. Mikada, T. Tsutsui, and F. Masutani (1997), Structure of the Kirishima volcanic region and its magma supply system (in Japanese), *Bull. Volcanol. Soc. Jpn.*, *S158*, S157–165.

Kanda, W., M. Utsugi, Y. Tanaka, T. Hashimoto, I. Fujii, T. Hasenaka, and N. Shigeno (2010), A heating process of Kuchi-erabu-jima volcano, Japan, as inferred from geomagnetic field variations and electrical structure, *J. Volcanol. Geotherm. Res.*, *189*, 158–171, doi:10.1016/j.jvolgeores.2009.11.002.

Kelbert, A., G. D. Egbert, and C. DeGroot-Hedlin (2012), Crust and upper mantle electrical conductivity beneath the Yellowstone Hotspot Track, *Geology*, *40*, 447–450, doi:10.1130/g32655.1.

Kozono, T., H. Ueda, T. Ozawa, T. Koyaguchi, E. Fujita, A. Tomiya, and Y. J. Suzuki (2013), Magma discharge variations during the 2011 eruptions of Shinmoe-dake volcano, Japan, revealed by geodetic and satellite observations, *Bull. Volcanol.*, *75*, 695, doi:10.1007/s00445-013-0695-4.

Lezaeta, P., and V. Haak (2003), Beyond magnetotelluric decomposition: Induction, current channeling, and magnetotelluric phases over 90 degrees, *J. Geophys. Res.*, *108*, 2305, doi:10.1029/2001JB000990.

Minakami, T., S. Utibori, M. Yamaguchi, N. Gyoda, T. Utsunomiya, M. Hagiwara, and K. Hirai (1969), The Ebino earthquake swarm and the seismic activity in the Kirishima volcanoes, in 1968–1969, part 1. Hypocentral distribution of the 1968 Ebino earthquakes inside the Kakuto caldera, *Bull. Earthquake Res. Inst. Univ. Tokyo*, *47*, 721–743.

Miyazaki, T., M. Yamaguchi, F. Masutani, and E. Terao (1976), The earthquake swarms in the northern area of the Kirishima volcanoes, 1975–1976, *Bull. Earthquake Res. Inst. Univ. Tokyo*, *51*, 115–149.

Moorkamp, M. (2007), Comment on "The magnetotelluric phase tensor" by T.Grant Caldwell, Hugh M. Bibby and Colin Brown, *Geophys. J. Int.*, *171*, 565–566, doi:10.1111/j.1365-246X.2007.03490.x.

Nakada, S., M. Nagai, T. Kaneko, Y. Suzuki, and F. Maeno (2013), The outline of the 2011 eruption at Shinmoe-dake (Kirishima), Japan, *Earth Planets Space*, *65*, 475–488.

Nakamichi, H., Y. Yamanaka, T. Terakawa, S. Horikawa, T. Okuda, and F. Yamazaki (2013), Continuous long-term array analysis of seismic records observed during the 2011 Shinmoedake eruption activity of Kirishima volcano, southwest Japan, *Earth Planets Space*, *65*, 551–562.

Nakao, S., Y. Morita, H. Yakiwara, J. Oikawa, H. Ueda, H. Takahashi, Y. Ohta, T. Matsushima, and M. Iguchi (2013), Volume change of the magma reservoir relating to the 2011 Kirishima Shinmoe-dake eruption—Charging, discharging and recharging process inferred from GPS measurements, *Earth Planets Space*, *65*, 505–515.

Nesbitt, B. E. (1993), Electrical resistivities of crustal fluids, *J. Geophys. Res.*, *98*, 4301–4310.

Ni, H. W., H. Keppler, and H. Behrens (2011), Electrical conductivity of hydrous basaltic melts: Implications for partial melting in the upper mantle, *Contrib. Mineral. Petrol.*, *162*, 637–650, doi:10.1007/s00410-011-0617-4.

Nurhasan, Y. Ogawa, N. Ujihara, S. B. Tank, Y. Honkura, S. Onizawa, T. Mori, and M. Makino (2006), Two electrical conductors beneath Kusatsu-Shirane volcano, Japan, imaged by audiomagnetotellurics, and their implications for the hydrothermal system, *Earth Planets Space*, *58*, 1053–1059.

Ogawa, Y., N. Matsushima, H. Oshima, S. Takakura, M. Utsugi, K. Hirano, M. Igarashi, and T. Doi (1998), A resistivity cross-section of Usu volcano, Hokkaido, Japan, by audiomagnetotelluric soundings, *Earth Planets Space*, *50*, 339–346.

Parkinson, W. D. (1962), The influence of continents and oceans on geomagnetic variations, *Geophys. J. R. Astron. Soc.*, *6*, 441–449, doi:10.1111/j.1365-246X.1962.tb02992.x.

Pek, J., and T. Verner (1997), Finite-difference modelling of magnetotelluric fields in two-dimensional anisotropic media, *Geophys. J. Int.*, *128*, 505–521, doi:10.1111/j.1365-246X.1997.tb05314.x.

Pous, J., W. Heise, P. A. Schnegg, G. Munoz, J. Marti, and C. Soriano (2002), Magnetotelluric study of the Las Canadas caldera (Tenerife, Canary Islands): Structural and hydrogeological implications, *Earth Planet. Sci. Lett.*, *204*, 249–263, doi:10.1016/s0012-821x(02)00956-1.

Seno, T., S. Stein, and A. E. Gripp (1993), A model for the motion of the Philippine Sea Plate consistent with NUVEL-1 and geological data, *J. Geophys. Res.*, *98*, 17,941–17,948, doi:10.1029/93JB00782.

Siniscalchi, A., S. Tripaldi, M. Neri, M. Balasco, G. Romano, J. Ruch, and D. Schiavone (2012), Flank instability structure of Mt. Etna inferred by a magnetotelluric survey, *J. Geophys. Res.*, *117*, B03216, doi:10.1029/2011JB008657.

Siripunvaraporn, W., and G. Egbert (2000), An efficient data-subspace inversion method for 2-D magnetotelluric data, *Geophysics*, *65*, doi:10.1190/1.1444778.

Siripunvaraporn, W., and G. Egbert (2009), WSINV3DMT: Vertical magnetic field transfer function inversion and parallel implementation, *Phys. Earth Planet. Inter.*, *173*, 317–329, doi:10.1016/j.pepi.2009.01.013.

Siripunvaraporn, W., G. Egbert, Y. Lenbury, and M. Uyeshima (2005), Three-dimensional magnetotelluric inversion: Data-space method, *Phys. Earth Planet. Inter.*, *150*, 3–14, doi:10.1016/j.pepi.2004.08.023.

Suzuki, Y., A. Yasuda, N. Hokanishi, T. Kaneko, S. Nakada, and T. Fujii (2013), Syneruptive deep magma transfer and shallow magma remobilization during the 2011 eruption of Shinmoe-dake, Japan—Constraints from melt inclusions and phase equilibria experiments, *J. Volcanol. Geotherm. Res.*, *257*, 184–204, doi:10.1016/j.jvolgeores.2013.03.017.

Tajima, H., and S. Aramaki (1980), Bouguer gravity anomaly around Kirishima volcanoes, Kyusyu, *Bull. Earthquake Res. Inst. Univ. Tokyo*, *55*, 241–257.

Tsutsui, M., K. Tomita, and T. Kobayashi (2005), Fumarolic Activity since December 2003 and Volcanic Activity during the Meiji and Taisho Eras (1880–1923) of Ohachi Volcano, Kirishima Volcano Group, Southern Kyushu, Japan, *Bull. Volcanol. Soc. Jpn.* (in Japanese with English abstract), *50*, 475–489.

Tyburczy, J. A., and H. S. Waff (1983), Electrical-conductivity of molten basalt and andesite to 25 kilobars pressure—Geophysical significance and implications for charge transport and melt structure, *J. Geophys. Res.*, *88*, 2413–2430, doi:10.1029/JB088iB03p02413.

Uchida, T., and Y. Sasaki (2006), Stable 3D inversion of MT data and its application to geothermal exploration, *Exploration Geophys.*, *37*, 223–230.

Ueda, H., T. Kozono, E. Fujita, Y. Kohno, M. Nagai, Y. Miyagi, and T. Tanada (2013), Crustal deformation associated with the 2011 Shinmoe-dake eruption as observed by tiltmeters and GPS, *Earth Planets Space*, *65*, 517–525.

Utada, H., T. Kagiyama, and EM-research-group-for-Kirishima-volcano (1994), Deep resistivity structure of Kirishima volcano (1), *Bull. Earthquake Res. Inst. Univ. Tokyo*, *69*, 241–255.

Worzewski, T., M. Jegen, H. Kopp, H. Brasse, and W. T. Castillo (2011), Magnetotelluric image of the fluid cycle in the Costa Rican subduction zone, *Nat. Geosci.*, *4*, 108–111, doi:10.1038/ngeo1041.

Yamamoto, K., and Y. Ida (1994), Three-dimensional P-wave velocity structure of Kirishima volcanoes using regional seismic events (in Japanese), *Bull. Earthquake Res. Inst. Univ. Tokyo*, *69*, 267–289.

Yamamoto, K., and Y. Ida (1997), Significant P wave attenuation for a specific frequency range beneath Kirishima Volcano, Japan, *Geophys. Res. Lett.*, *24*, 1275–1278, doi:10.1029/97GL01157.

Yamaya, Y., T. Mogi, T. Hashimoto, and H. Ichihara (2009), Hydrothermal system beneath the crater of Tarumai volcano, Japan: 3-D resistivity structure revealed using audio-magnetotellurics and induction vector, *J. Volcanol. Geotherm. Res.*, *187*, 193–202, doi:10.1016/j.jvolgeores.2009.09.008.